Developmental regulation of active and passive membrane properties in rat vibrissa motoneurones

Quoc-Thang Nguyen[1], Ralf Wessel[3] and David Kleinfeld[1,2]

[1]*Department of Physics and* [2]*Graduate Program in Neurosciences, University of California at San Diego, La Jolla, CA 92093 USA*
[3]*Department of Physics, Washington University, St Louis, MO 63130 USA*

We characterized the electrophysiological properties of vibrissa motoneurones (vMNs) in rat. Intracellular recordings of vMNs in brainstem slices from animals aged P4 to P5 and P9 to P11, i.e. newborn animals, showed that the subthreshold membrane impedance has the form of passive decay. In particular, the impedance follows the $1/\sqrt{f}$ signature for long dendrites beyond a cut-off frequency of $f_c = 8$ Hz. In contrast, the impedance has the form of a resonant filter in vMNs from slices prepared from animals aged P17 to P23, i.e. young animals. The resonance has a peak near 4 Hz and an amplitude of 1.2 times that at low frequencies ($f \sim 0.1$ Hz). The low frequency onset of the resonance is shown to depend on a hyperpolarization-activated depolarizing current, I_h. This current functions as a high-pass filter. The high frequency cut-off of the resonance results from passive decay in long dendrites, similar to the case with newborn animals but with $f_c = 20$ Hz. In addition to a resonance in subthreshold properties, an enhanced resonance in spiking is observed in young as opposed to newborn animals. The transition from solely passive decay in vMNs from newborn animals to resonance in young animals coincides with the onset of whisking. Further, the width of the resonance encompasses the 4–15 Hz range of exploratory whisking. Nonetheless, it remains to be shown if there is a causal relation between the regulation of currents in vMNs and the onset of whisking. In particular, we further observed that the membrane impedance of hypoglossal motoneurones from both newborn and young animals exhibits a subthreshold resonance that also peaks near 4 Hz. The amplitude of this resonance increases from 1.1 to 1.4 times that at low frequencies in newborn *versus* young animals. We conjecture that resonance properties in vibrissa, hypoglossal, and potentially other motoneurones, may serve to transiently and purposely synchronize different orofacial behaviours.

(Resubmitted 23 December 2003; accepted after revision 30 January 2004; first published online 6 February 2004)
Corresponding author D. Kleinfeld: Department of Physics and Graduate Program in Neurosciences, University of California at San Diego, La Jolla, CA 92093, USA. Email: dk@physics.ucsd.edu

The rat vibrissa sensorimotor system has emerged as a major experimental system to study active tactile sensation (reviewed in Kleinfeld *et al.* 1999, and Mehta & Kleinfeld, 2004). The final common path for the motor control of the vibrissae, the large facial hairs used for sensation, is provided by motoneurones of the facial nucleus (cranial nucleus VII). The facial nucleus is located in the medulla and is part of an anatomical loop that consists of the facial muscles, which provide force to move the vibrissae, the trigeminal ganglion, which innervates the vibrissa follicles and receives sensory information from vibrissae movement, and the trigeminal sensory nuclei, which mediate feedback to the facial nucleus and also project to pontine–cerebellar and thalamocortical regions (Fig. 1*A*). Further, the motoneurones in the facial nucleus integrate excitatory, inhibitory and modulatory inputs from a multitude of medullary, midbrain, and pontine premotor nuclei (Fig. 1*A*) (Hattox *et al.* 2002). Nuclei in the medulla and midbrain provide indirect paths for projections from primary motor cortex to the facial nucleus (Miyashita *et al.* 1994; Hattox *et al.* 2002).

In view of the integrative role of vibrissa facial motoneurones (vMNs) in the vibrissa sensorimotor pathway, there is a surprising paucity of data addressing the electrophysiological characteristics of these cells in relation to development. In particular, rats exhibit only small motions of their vibrissae shortly after birth. However, by postnatal day 13–15 they begin to whisk vigorously as they use their vibrissae to explore their spatial environment (Welker, 1964). During exploratory whisking, the motion of vibrissae is largely periodic and characterized by a frequency ranging from 4 to 15 Hz, with a centre frequency

 DOI: 10.1113/jphysiol.2003.060087

for all whisking events varying between 6 and 9 Hz (Welker, 1964; Carvell *et al.* 1991; Berg & Kleinfeld, 2003) (Table 1). We thus asked whether the development of active and passive membrane properties of vMNs could be related to the rhythmic nature and developmental time course of whisking.

Our experimental approach was to compare the intracellular response of vMNs to both constant and

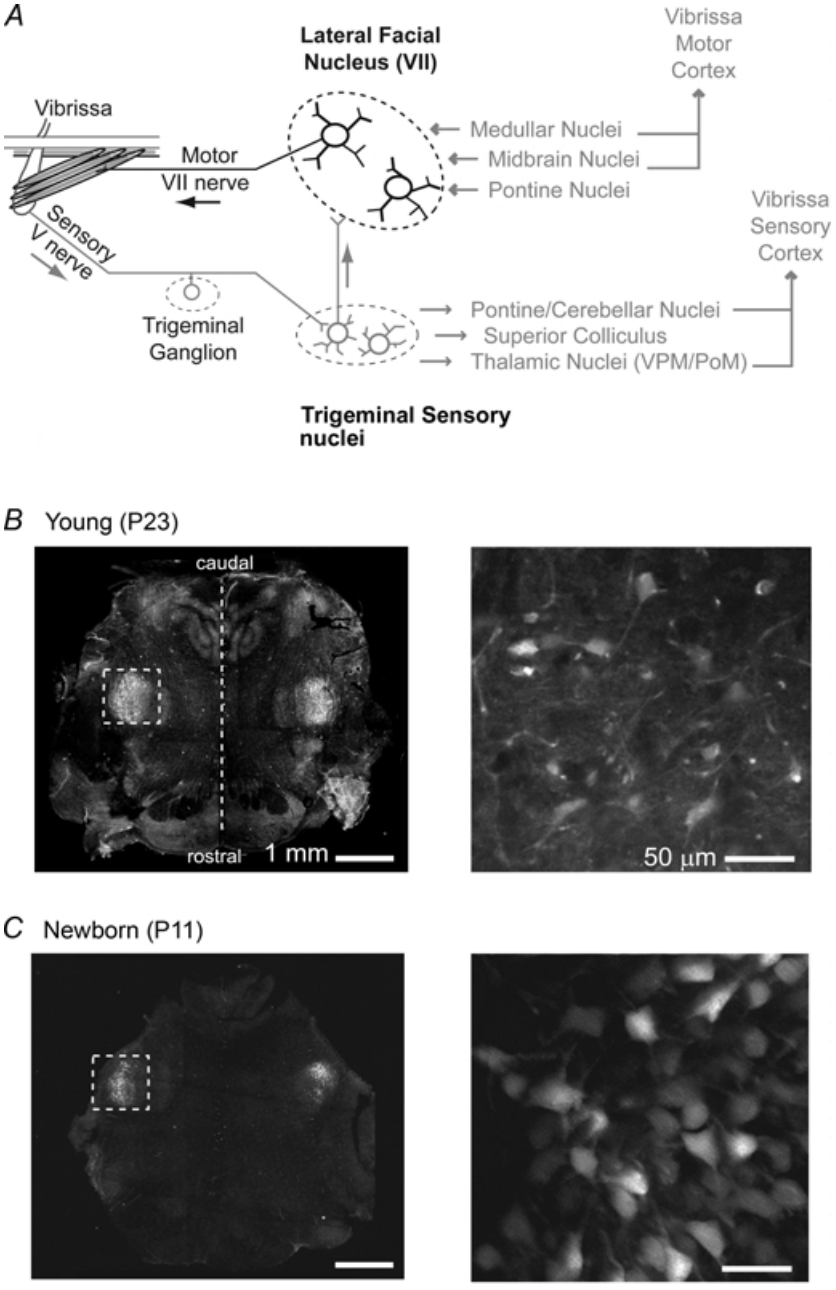

Figure 1. Functional anatomy of the facial nucleus and localization of vibrissa motoneurones
A, summary of afferent and efferent projections to and from the facial nucleus (Rekling *et al.* 2000; Hattox *et al.* 2002). *B*, confocal images of retrogradely labelled vMNs in horizontal brainstem slices from a P17 to P23 (P23) rat. *C*, confocal images of retrogradely labelled vMNs in horizontal brainstem slices from a P4 to P11 (P10) rat. In both rats the fluorescent dye Evans Blue was injected bilaterally into the mystacial pads resulting in bilateral labelling of the facial nucleus. In *B* and *C* the low magnification view is a single section while the higher magnifications are maximal projections through a depth of 20 μm for the right-hand panels. In the low magnification views, patches of high background fluorescence outside the region of the facial nucleus result from mounting artifacts.

Table 1. Frequencies of whisking in the rat

Whisking Behaviour	Center (Hz)	Range[1] (Hz)	Method[2]	Reference
Exploratory[3]	8	—	EMG	Hamada *et al.* 1999
Exploratory in air[4]	9	7–13	PDF of EMGs	Berg & Kleinfeld, 2003
Foveal[5]	—	12–22		
Exploratory in air	9	4–15	Power of EMG	O'Connor *et al.* 2002
Exploratory in air	8	5–13	Power of EMG	Fee *et al.* 1997
Exploratory	8	6–11	Cinematography	Welker, 1964
Exploratory	7	6–9	Power of EMG	Carvell & Simons, 1996
Exploratory	6	5–8	Power of EMG	Carvell & Simons, 1995
Foveal	—	15–22		
Exploratory	8	7–9	Power of EMG	Carvell *et al.* 1991
Exploratory	—	7–12	Videography	Nicolelis *et al.* 1995
Exploratory	7	6–8	EMG	Semba & Komisaruk, 1984
Head-fixed[6]	5	4–8	Power of 1D video	Gao *et al.* 2001
Average Exploratory	5–9	4–15		

[1]Given as the full range of values reported. [2]EMG (electromyogram from mystacial musculature); cinematography/videography (image rates of approximately 60 Hz); 1D video (single line scan videography at 2 kHz); Power (power spectrum); PDF (probability distribution function, computed from the peak values of power spectra). [3]Exploratory whisking, the most common behaviour, refers to large amplitude whisks with set-points near midrange angles. [4]Exploratory whisking in air refers to large amplitude whisks with the rat perched so that the vibrissa make no contact. [5]Foveal whisking occurs when a rat thrusts its vibrissae forward to contact and palpate a distant object, such as when a rat cranes across a gap (Berg & Kleinfeld, 2003). [6]Whisking in air under operant conditioning.

time-varying currents in newborn animals, i.e. postnatal days 4–11, with young animals, i.e. postnatal days 17–23. We focused on membrane resonance, i.e. the selective increase of membrane impedance and spiking rate for inputs at preferential frequencies. These phenomena have been proposed as a possible mechanism to generate neuronal rhythms in defined frequency bands (reviewed in Hutcheon & Yarom, 2000) and speculated to facilitate phase-locking among populations of neuronal oscillators (Izhikevitch, 2001). We thus conjectured that vMNs in brainstem may also function as band-limited filters that regulate the frequency-rich drive signals to the mystacial musculature. As a control for the possible uniqueness of the development of electrophysiological properties of vMNs, we further looked at the electrophysiological properties of hypoglossal motoneurones in relation to development, building on the work of Viana *et al.* (1994).

Methods

Retrograde labelling of vMNs

Facial motoneurones that innervate muscles in the mystacial pad of newborn and young rats were routinely labelled with the retrogradely transported, fluorescent dye Evans Blue (Takahashi, 1990). Rats were anaesthetized by halothane inhalation, and 20–30 μl of 2% (w/v) Evans Blue dissolved in phosphate buffered saline (PBS) was injected in the mystacial pad. Animals were used 1–3 days after injection. The care and all aspects of experimental manipulation of our animals were in strict accordance with guidelines from the National Institutes of Health and were approved by the UCSD Institutional Animal Care and Use Committee.

Slice preparation and solutions: facial nucleus

Horizontal slices of brainstem that contained the facial nucleus were obtained from Sprague–Dawley rats as described (Aghajanian & Rasmussen, 1989). In brief, rats were deeply anaesthetized by halothane inhalation, decapitated and the brain was immediately immersed in ice-cold, low-sodium artificial cerebrospinal fluid (ACSF; 220 mM sucrose, 2.5 mM KCl, 3 mM $MgSO_4$, 26 mM $NaHCO_3$, 1.25 mM NaH_2PO_4, 1 mM $CaCl_2$ and 10 mM D-glucose) that was bubbled with carbogen (95% O_2 and 5% CO_2) for final values of pH 7.35–7.40 and 310 mosmol l^{-1}. The brainstem was removed from the cranium and the cerebellum dissected out. The brainstem was then trimmed and glued to a tissue dish with the fourth ventricle down. Horizontal sections were cut on a Vibratome 1000 (Ted Pella Inc., Redding, CA, USA) at a thickness of 300 μm and were incubated for at least 1 h at 32°C in ACSF (126 mM NaCl, 5 mM KCl, 2 mM $MgSO_4$, 26 mM $NaHCO_3$, 1.25 mM NaH_2PO_4, 2 mM $CaCl_2$ and 10 mM D-glucose bubbled with carbogen) that was supplemented with 3 mM *myo*-inositol, 2 mM pyruvate, 0.5 mM ascorbic acid and 4 mM lactic acid (Takahashi *et al.* 2000). For patch-clamping of motoneurones from P15–P23 animals, slices were treated with 0.5–1 mg ml^{-1} pronase (Calbiochem, San Diego, CA, USA), added to the incubation solution, for at least 1 h. For recording, slices were transferred

to a chamber (RC22C, Warner, New Haven, CT, USA), perfused with ACSF at a flow of 2 ml min^{-1} and at a temperature of 32°C, and visualized by an upright microscope equipped with a ×40 water immersion objective, DIC optics and video observation (C2400-79 CCD camera, Hamamatsu, Bridgewater, NJ, USA).

Slice preparation: hypoglossal nucleus

Slices of brainstem that contained the hypoglossal nucleus were obtained from young and newborn Sprague–Dawley rats as described in Viana *et al.* (1994). We prepared 300–400 μm-thick coronal sections. All other procedures were the same as with slices containing the facial nucleus.

Electrophysiology

Sharp borosilicate microelectrodes (1 mm o.d. and 0.75 mm i.d., A-M Systems, Carlsborg, WA, USA) were pulled on a horizontal puller (P-80; Sutter Instruments, Novato, CA, USA) and filled with 3 M KCl. Electrodes had initial resistances of 40–100 MΩ. Current-clamp recordings were made with an Axoclamp 2A amplifier (Axon Instruments, Union City, CA, USA). Cell input resistances were determined from measurements of the voltage change in response to 0.1–0.3 nA step current injections. Whole-cell recordings were achieved with patch electrodes pulled from 7052 glass (1.5 mm o.d., 1.2 mm i.d.; Garner Glass, Claremont, CA, USA) and filled with 100 mM potassium gluconate, 40 mM KCl, 10 mM Hepes buffer, 2 mM $MgCl_2$, 2 mM Mg-ATP, 1.1 mM EGTA, and 0.1 mM $CaCl_2$, adjusted to pH 7.2. Patch pipettes had a resistance of 3–6 MΩ in the bath and a series resistance between 8 MΩ and 30 MΩ in the whole-cell configuration. Junction potentials were not corrected. Recordings were performed with an Axopatch 200B amplifier (Axon Instruments) operated in current-clamp mode. All chemicals were from Sigma, except ZD-7288 which was purchased from Tocris Cookson (Ellisville, MO, USA).

Stimulus waveform generation and data logging utilized a standard computer interface (PCI-MIO 6024E, National Instruments, Austin, TX, USA) and either programs of local design written in LabView (National Instruments) or the WinWCP software (courtesy of Dr J. Dempster, University of Strathclyde, UK). Statistical significance between properties of P17 to P23 and P4 to P11 vMNs was assessed using Student's two-tailed unpaired *t* test.

Histology

Neurones that were filled with biocytin were processed as described (Thurbon *et al.* 1998). In brief, slices were fixed by immersion in 4% (w/v) paraformaldehyde in PBS overnight, equilibrated with 30% (w/v) sucrose in PBS for 24 h, and incubated in 1% (w/w) Triton X-100 with an avidin–biotin complex (ABC Elite kit, Vector Laboratories, Burlingame, CA, USA) for 16 h at 5°C. The reaction product was visualized with 3,3′-diaminobenzidine. Filled neurones were localized at the light microscope level and the projections across multiple sections were drawn and reconstructed with a camera lucida attachment. Motoneurones retrogradely labelled with Evans Blue were observed under a MRC-1024 confocal microscope (Bio-Rad, Hercules, CA, USA) using the $\lambda = 532$ nm argon excitation line and a $\lambda = 580$ nm dichroic mirror.

Results

Anatomy

We used horizontal slices of brainstem for our recordings (Methods) to conserve as much as possible the dendritic arborization of facial motoneurones which extends generally in a rostro-caudal direction (Friauf, 1986). To confirm the localization of vibrissa motoneurones (vMNs) within the facial nucleus, we injected the retrogradely transported dye Evans Blue in both mystacial pads and mapped the distribution of labelled cells in the slice. Confocal imaging of fixed slices from young and newborn rats revealed large, retrogradely labelled neurones in the lateral division of the facial nuclei on both sides of the slice (Fig. 1*B* and *C*). Their location agreed with that found in previous studies (e.g. Hattox *et al.* 2002).

The above mapping allowed us to use light microscopy at low magnification to locate the facial nucleus as a grey region from which fibres emerged and ran towards the midline. Electrodes were positioned in the lateral aspect of the facial nucleus where clusters of large, multipolar cells could be observed with high magnification, differential interference contrast optics, and video enhancement. These cells were targeted for impalement with glass microelectrodes. The identity and location of recorded cells was subsequently confirmed by *post hoc* biocytin fills. Based on their morphology and on the apparent absence of interneurones in the facial nucleus (bounded at <2% of the total population; McCall & Aghajanian, 1979), all recorded cells were presumed to be vibrissa motoneurones.

Basic electrophysiology

We consider first the electrophysiological parameters of vMNs in young, intermediate and newborn rats

Table 2. Basic electrophysiological parameters of vMNs (means ± S.D.)

		Newborn		Intermediate	Young
		(P4 to P5)	(P9 to P11)	(P12 to P16)	(P17 to P23)
V_{rest} (mV)	Sharp	—	−66 ± 7 (34)	−66 ± 5 (17)	−68 ± 6 (39)
	Patch	−62 ± 6 (12)	—	—	−60 ± 11 (10)
R_m (MΩ)	Sharp	—	30 ± 12 (33)*	22 ± 9 (17)	24 ± 12 (35)*
	Patch	148 ± 106 (12)	—	—	115 ± 58 (10)
τ_m (ms)	Sharp	—	9 ± 3 (14)	7.5 ± 2.1 (7)	9 ± 4 (20)
	Patch	35 ± 3 (12)	—	—	13 ± 3 (10)
I_{rheo} (nA)	Sharp	—	0.5 ± 0.2 (32)*	0.7 ± 0.3 (16)	0.6 ± 0.3 (34)*
ρ	Patch	20 (12)	—	—	20 (10)
L/λ	Patch	1.4 ± 0.3 (3)	—	—	1.1 ± 0.2 (8)

Statistically different ($P < 0.05$). V_{rest}: resting membrane potential. R_m: membrane resistance. τ_m: membrane time constant. I_{rheo}: current rheobase. ρ: ratio of dendritic to somatic conductances. L/λ: normalized electrotonic length. (*n*): sample size of individual neurones. –: not measured

recorded with sharp microelectrodes (Table 2). The resting membrane potential was on average the same in all age groups. The input resistance was statistically smaller in vMNs from young as compared to newborn animals; we will return to this issue in the context of recordings with patch microelectrodes. Fast spikes elicited by the injection of a step of depolarizing current could be observed in vMNs from all postnatal age groups as well as in vMNs from neonates as young as P2 ($n = 5$ cells; data not shown). There was a marginal, although significantly higher, current threshold for spike generation in vMNs from young animals, consistent with their lower input resistance (Table 2). All of the action potentials seen in vMNs could be reversibly blocked by 500 nM tetrodotoxin (TTX). Therefore we assumed that they were mediated by TTX-sensitive, voltage-activated sodium channels.

The depolarization-triggered spikes were followed by fast and slow after-hyperpolarization potentials in all age groups. Subsequent to a train of action potentials, 5–18 Hz subthreshold oscillations similar to those described by Magariños-Ascone *et al.* (1999) were observed in 44% of the cells from P17 to P23 animals ($n = 36$) and 28% of the cells from P4 to P11 animals ($n = 32$). Injection of a hyperpolarizing current pulse usually led to a hyperpolarization with a transient component that slowly decayed toward a baseline value. This transient is denoted a voltage sag. Lastly, miniature excitatory postsynaptic potentials were resolved in all age groups. These data indicate that excitatory inputs to vMNs were presumably functional before, during and after the onset of whisking.

Suprathreshold step response

When several spikes were generated by the injection of a step of current, usually with an amplitude that exceeded ∼1 nA, the spike pattern was that of an initial doublet of action potentials with short interspike interval followed by a train of action potentials with either a sustained or a decreasing interspike interval (Fig. 2*A*). These types were seen in all age groups of vMNs and correspond to type I (sustained spiking) or type II (adapting) motoneurones, respectively (Magariños-Ascone *et al.* 1999). An increase in the stimulus amplitude attenuated the spike-frequency adaptation and increased the average spike rate in vMNs from all age groups.

To determine the gain curve, or frequency *versus* injected current, the membrane potential of vMNs was routinely set at −65 mV, which is approximately the resting potential of vMNs (Table 2). Although the first interspike frequency remained comparable in vMNs from young and newborn rats for all current amplitudes (gain ∼82 Hz nA^{-1}; Fig. 2*B*), the average spiking rate of newborn vMNs became significantly larger than that of young vMNs as stimulus amplitude increased from 1.1 to 1.4 nA (gain ∼28 and 18 Hz nA^{-1} for newborn and young animals, respectively; Fig. 2*C*).

Subthreshold membrane impedance

The frequency dependence of the subthreshold membrane impedance provides the baseline dynamics for the integration of synaptic inputs by vMNs. The impedance is a complex function of frequency that is defined by:

$$Z(f) = \frac{V_m(f)}{I_{inject}(f)}$$

It was determined experimentally by injecting subthreshold sinusoidal currents into vMNs, of the form $I_{inject}(f) = \Delta I \sin(2\pi ft)$ over a range of frequencies, denoted f. Measurement of the resulting sinusoidal voltage change, $V_m(f) = \Delta V_m(f)\sin(2\pi ft + \phi)$, was

used to deduce the magnitude of $Z(f)$, given by $|Z(f)| = \Delta V_m(f)/\Delta I$, and the phase of $Z(f)$, given by ϕ (left panel, Fig. 3*a*). The average membrane potential, denoted V_0, was varied by the addition of the constant level of injected current.

We consider first various examples of $V_m(f)$ for three different stimulation frequencies with the amplitude of $I_{inject}(f)$, ΔI, held fixed. In a vMN from a young animal, with average membrane potentials of either $V_0 = -80$ and -70 mV, the amplitude of the sinusoidal voltage, $\Delta V_m(f)$, was larger for currents at $f = 4$ Hz than at either $f = 0.2$ or 20 Hz (left panel, Fig. 3*A*). This heightened response at an intermediate frequency is indicative of a resonant behaviour. The voltage response of a vMN from an intermediate aged animal exhibited resonant behaviour only at the hyperpolarizing average potential of $V_0 = -80$ mV and low-pass behaviour at the higher average potential of $V_0 = -70$ mV (middle panel, Fig. 3*A*). Lastly, in a vMN from a newborn animal, the amplitude of $\Delta V_m(f)$ decreased as a function of increasing frequency

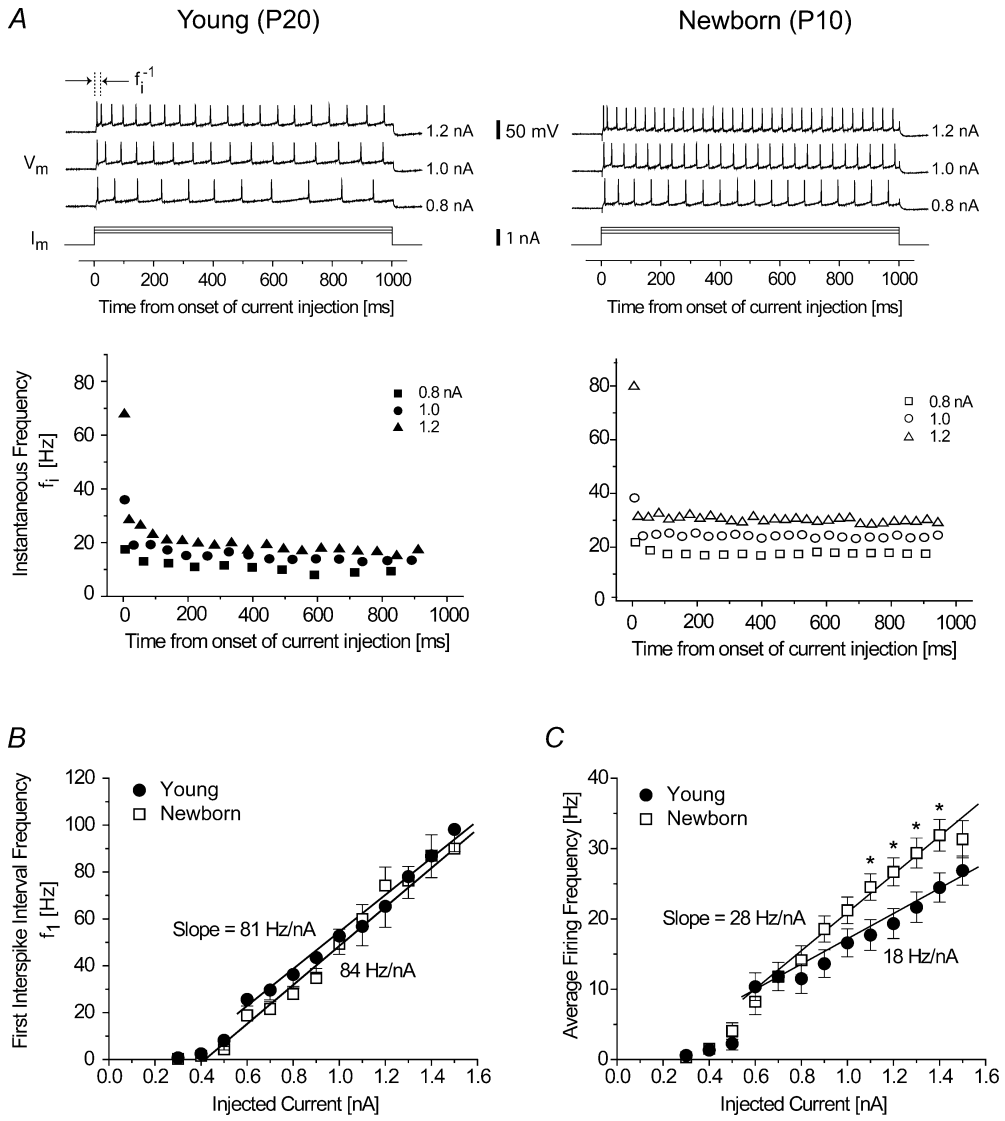

Figure 2. Responses of vMNs from P17 to P23 and P4 to P11 animals in response to injection of a suprathreshold current step

A, upper traces, spike trains elicited by 1 s current injections in a cell from P20 animal and one from a P10 animal. Lower Traces, instantaneous firing frequency for the same cells. *B*, first interspike frequency of vMNs (n = 10–24 cells per point from P17 to P23 animals and n = 14–27 cells per point from P4 to P11 animals). The error bars represent 1 S.E.M. *C*, average firing frequency for the same cells as in *B*. The asterisk signifies that the firing frequencies for vMNs from P17 to P23 *versus* P4 to P11 animals are statistically different ($P < 0.05$).

at both $V_0 = -80$ mV and -70 mV (right panel, Fig. 3*A*). Thus, the voltage dependencies in this cell, unlike cells from young rats, were consistent with a passive, low-pass response.

The full frequency dependence of the membrane impedance was determined over the range $0.1 \leq f \leq 100$ Hz as an average over individual measurements across our sample of slices and cells. Since there was variability in the membrane resistance between different neurones (Table 2 with $Z(0) = (R_m)$, we plot the normalized quantity $|Z(f)|/|Z(f = 0.1\,\text{Hz})|$. We consider here only the magnitude of the impedance; the phase will be discussed in a later section on the cable properties of the impedance. Data were obtained with average membrane potentials in the range $-80\,\text{mV} \leq V_0 \leq -60\,\text{mV}$. For average potentials $V_0 < -65$ mV, the magnitude of the impedance for vMNs from young animals ($n = 6$–25 cells per data point) exhibited a broad peak that was centred at 4 Hz and rolled off at high frequencies (Fig. 3*B*, left panel). The amplitude of resonance, denote Q, increased with increasing hyperpolarization and reached a maximum value of $|Z(f)|/|Z(f = 0.1\,\text{Hz})| = 1.23$ at

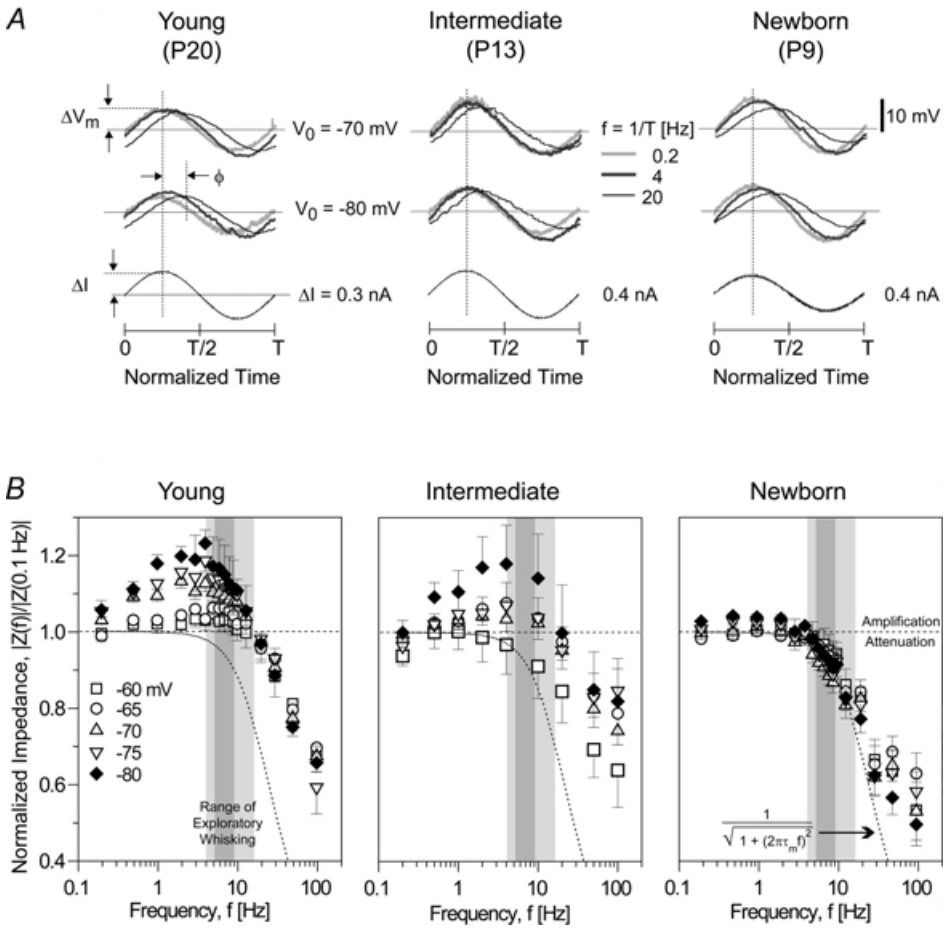

Figure 3. Voltage-dependence and developmental regulation of the subthreshold resonance
A, membrane potentials during the injection of a subthreshold sinusoidal current at 0.2, 4 and 20 Hz in a P20 (left traces), P13 (middle traces) and a P9 (right traces) vMN at DC potentials of $V_0 = -70$ mV and -80 mV. Responses to single cycles are superimposed to emphasize the increase of the phase shift at 20 Hz. Current amplitude was 0.4 nA for the motoneurones from P13 and P20 animals and 0.3 nA for the neurone from the P9 animal. *B*, normalized amplitude of the membrane impedance for vMNs in P17 to P23 (left graph), intermediate (middle graph) and P4 to P11 (right graph) animals. The membrane potentials varied between -60 mV and -80 mV. The normalized amplitude at -80 mV is significantly larger than the corresponding values at -60 mV ($P < 0.01$). The error bars represent 1 S.E.M. The dark grey band represents the range of centre frequencies for whisking and the light grey band represents the full range of frequencies observed during whisking (Table 1). Dotted lines are plots of the normalized amplitude of the membrane impedance of electrically compact cells with time constants τ_m corresponding to the values found with sharp electrodes in Table 2 (see text for details).

$V_0 = -80$ mV. Vibrissa motoneurones in the intermediate age group ($n = 3$–11 cells) also displayed a resonance in the membrane impedance, albeit with a smaller peak values for each average voltage level (Fig. 3*B*, middle panel). In contrast to the case for animals that whisk, the magnitude of the normalized impedance in vMNs from newborn animals (n = 10–24 cells) decreased monotonically with increasing frequencies for all membrane potentials (Fig. 3*B*, right panel). *In toto*, these data show a clear correlation between the maturation of whisking and the presence of a membrane resonance in vMNs. Lastly, membrane impedance decreased at high frequencies (>19 Hz for young and intermediate vMNs, > 5 Hz for newborn vMNs). If vMNs were electrically compact, they would have a normalized membrane impedance amplitude equal to $(1 + (2\pi\tau_m f)^2)^{-1/2}$ where τ_m is the measured time constant of the membrane (Table 2). We note that the behaviour of the membrane impedance of vMNs at high frequency did not fit this assumption, but rather decays more slowly (Fig. 3*B*); we will return to this issue.

Ionic contribution to the resonance

Most vMNs from young and newborn animals displayed a sag voltage response when stimulated with constant, hyperpolarizing currents. We quantified the relation between the amplitude of the sag and the magnitude of the peak of the resonance. The relative contribution of the sag response was determined from the measured peak, p, and steady-state, s, values of the voltage measures in response to a −1.5 nA step of current (Fig. 4*A*). We define the 'sag ratio', denoted SR, as

$$\mathrm{SR} \equiv \frac{\mathrm{p} - \mathrm{s}}{\mathrm{p}} = 1 - \frac{\mathrm{s}}{\mathrm{p}}$$

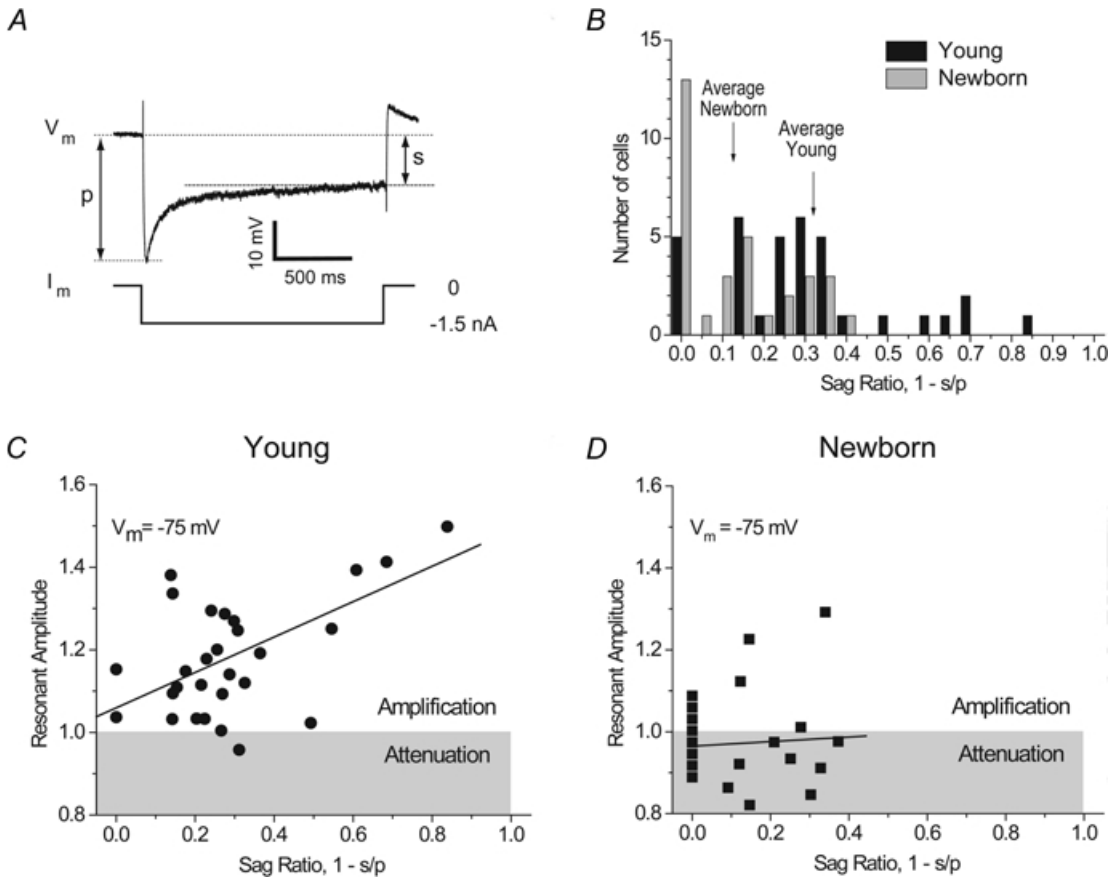

Figure 4. Phenomenology of the sag current in young and newborn vMNs
A, typical voltage response after the injection of a step of current. This response is used to define a sag ratio and used to find the decay time of the sag response. *B*, distribution of sag ratios for young ($n = 35$) *versus* newborn ($n = 32$) cells. Bin size: 0.05. *C*, correlation between the sag ratio and the normalized amplitude of membrane impedance at 4Hz and $V_0 = -75$ mV for young cells ($n = 28$). *D*, correlation between the sag ratio and the normalized amplitude of membrane impedance at 4Hz and $V_0 = -75$ mV for newborn cells ($n = 20$).

The distribution of sag ratios showed an increase toward larger values when animals developed from the P4 to P11 to the P17 to P23 stage (Fig. 4*B*). The value of the sag ratio was significantly ($P < 0.005$) larger in vMNs from young *versus* newborn animals (Fig. 4*B*), i.e. SR = 0.27 ± 0.22 (mean ± S.D.; $n = 33$ cells) *versus* SR = 0.12 ± 0.12 ($n = 32$ cells) for vMNs from young *versus* newborn animals, respectively. The amplitude of the resonance in young vMNs, measured at 4 Hz and $V_0 = -75$ mV, was significantly correlated with the sag ratio ($r = 0.53$ with $P < 0.005$) (Fig. 4*c*). In young vMNs, small sag ratios were sometimes recorded without an associated resonance because in general hyperpolarization with current pulses was much larger than the voltage swings induced by sinusoidal current injection. No significant correlation was observed between the amplitude of a possible subthreshold resonance and the sag ratio in cells from newborn animals (Fig. 4*D*), as expected. Lastly, the decay of the sag was best fitted with one exponential and a small, linear component. The time constant of the exponential, referred to as the sag response decay, was 0.18 ± 0.11 s (mean ± S.D., $n = 27$) and 0.30 ± 0.19 s ($n = 14$) for cells from young and newborn animals, respectively.

We hypothesized that the subthreshold resonance depended on the hyperpolarization-activated cation current, I_h. To test this hypothesis, we applied pharmacological inhibitors of I_h on the membrane resonance in vMNs. The effect of pharmacological manipulation of the sag current is illustrated through a set of voltage responses to injections of depolarizing and hyperpolarizing currents for the particular example of a vMN from a P22 animal (Fig. 5*A*). Bath application of 4 mM CsCl, where Cs^+ is a blocker of I_h in facial motoneurones (Larkman & Kelly, 1998), suppressed the hyperpolarization-induced voltage sag within 6 min of the onset of superfusion. The blockage was partially restored after a 15 min wash-out of the CsCl. Subsequent application of the specific I_h blocker ZD-7288 (4-(*N*-ethyl-*N*-phenylamino)-1,2-dimethyl-6-(methylamino)pyrimidinium chloride; Larkman & Kelly, 2001), at a concentration of 20 μM, removed the voltage sag within 10 min after the onset of superfusion (Fig. 5*a*). In general ($n = 7$ cells) superfusions with 2–4 mM caesium completely abolished the resonance at either $V_0 = -70$, −75 or −80 mV (Fig. 5*B*, left graph). The resonance showed near full recovery after 15−30 min of washout (data not shown). Similarly, superfusion with 10−100 μM of ZD-7288 ($n = 6$ cells) completely suppressed the subthreshold resonance at all voltages studied (Fig. 5*B*, middle graph). Since the effect of ZD-7288 is practically irreversible in facial nucleus motoneurones (Larkman & Kelly, 2001), we did not attempt to observe if the resonance recovered after wash-out of the free ZD-7288.

We further tested whether the resonance was dependent on the potassium inward rectifier current I_{Kir} ($n = 6$ cells). Application of 1 mM Ba^{2+}, a blocker of I_{Kir}, increased the membrane resistance of vMNs (40% at −80 mV; data not shown) but did not have any appreciable effect on the membrane resonance at all voltages (Fig. 5*B*, right graph). Lastly, we tested whether the resonance was mediated by TTX-sensitive, voltage-activated sodium channels ($n = 2$ cells). We observed that perfusion with 1 μM TTX did not significantly affect the membrane resonance (data not shown). We thus conclude that the hyperpolarization-activated cation current I_h is a necessary component of the resonance.

Cable properties of vMNs

As mentioned previously, the low-pass filtering observed at high frequencies in all age groups is not consistent with vMNs being electrically compact. *Post hoc* histology of biocytin-filled neurones revealed the existence of extensive dendritic trees in vMNs from all age groups (Fig. 6*A*) consistent with previous anatomical work (Friauf, 1986). There was no significant difference in the distribution of dendritic branch lengths in newborn and young vMNs (Fig. 6*B*) (Kolmogorov-Smirnoff test, $P < 0.05$). The somatic and dendritic morphological parameters of the vMNs, summarized in Table 3, show that the mean length from the soma to the distal ends was roughly 130 μm, comparable with the typical scale of one electronic decay length (Turner & Schwartzkroin, 1983). We thus explored if the branching structure contributed to the low-pass filtering properties of the neurones, in particular if the frequency dependence of the impedance followed a $Z(f) \propto 1/\sqrt{f}$ dependence for long cables *versus* a $Z(f) \propto 1/f$ fall-off for compact cells (Jack *et al.* 1983). Whole-cell recordings were made with patch rather than sharp microelectrodes, since the latter can introduce a somatic shunt that will compromise measurements of the impedance in cells that are heavily branched (Durand, 1984). As patch-clamping cells from P17 to P23 animals is complicated by mature glia and connective tissue (Larkman & Kelly, 1995), slices were mildly treated with the enzyme pronase in order to obtain seal resistances greater than 1 GΩ in visually identified young motoneurones. In contrast, patch-clamp recordings of vMNs from newborn rats aged P3 to P5 were performed without enzymatic treatment.

Whole-cell patch-clamped vMNs from both young and newborn rats generated repetitive, overshooting

action potentials upon suprathreshold current injection (Fig. 6*C*). The average resting potentials were close to the values measured with sharp electrodes (Table 2). Consistent with the expectations for patch *versus* sharp electrodes, the membrane resistance was much higher for the patch measurements. The normalized amplitude and phase of the membrane impedance obtained in current-clamp decreased monotonically with frequency (Fig. 6*D*). At variance with our sharp electrode recordings, the patch recordings revealed little or no resonance in vMNs from young animals with V_0 in the range of −75 to −60 mV, with small or no sag responses. The losses of sag response and resonance in young vMNs are consistent with the disappearance of I_h observed when neurones are treated by proteolytic enzymes for patch recordings (Budde *et al.* 1994), and with a reduced concentration of metabolites necessary to activate I_h as a result of dialysis of the cell cytoplasm during the whole-cell recordings (Major *et al.* 1994). This fortuitous loss of I_h in young vMNs allowed us to delineate the frequency dependence of their passive membrane impedance.

We characterized the cable properties of the vMNs with models of increasing complexity. In the first model, we approximated a motoneurone as an isopotential R-C circuit that represents the cell soma, in parallel with a semi-infinite passive cable that mimics the dendrites (Rall, 1960). In the second model, we allowed the cable to have a finite length. The impedance of the circuit for the first model, normalized to the value at $f = 0$ Hz, can be derived from equation 7.74 in Jack *et al.* (1983), i.e.

$$Z(f) = R_m \frac{\rho + 1}{\left(\rho + \sqrt{1 + i2\pi f \tau_m}\right)\sqrt{1 + i2\pi f \tau_m}}$$

where ρ is the ratio between the resistance of the soma and that of the dendrites. When ρ is large, the measured impedance is dominated by the contribution of the semi-infinite cable and $Z(f) \propto (1 + i2\pi f \tau_m)^{-1/2}$. The amplitude of $Z(f)$ should decrease as $f^{-1/2}$, as the frequency is increased while the phase shift will be close to $-\pi/4$ at high frequencies. As the amplitude and phase of the membrane impedance showed little variation with the average potential, the patch-clamp data from all recordings

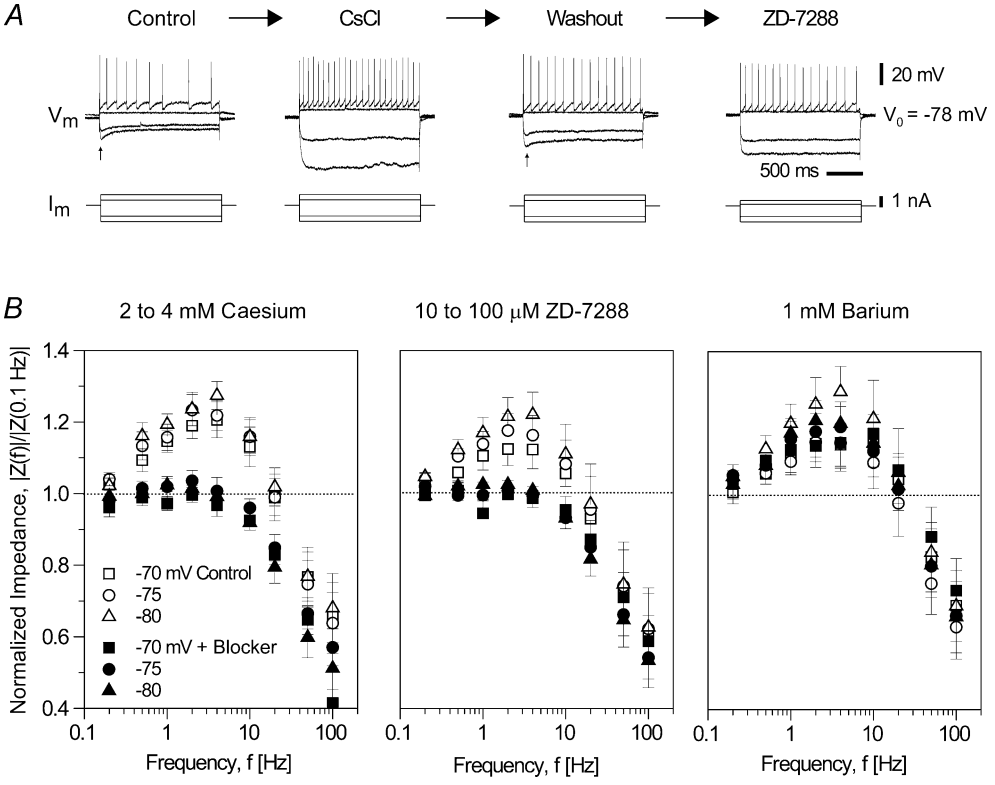

Figure 5. The ionic basis of the subthreshold membrane resonance in young vMNs
A, effects of 4 mM caesium and 20 μM ZD-7288 on the hyperpolarization-activated voltage sag in the same cell. Arrows indicate the onset of the sag. *B*, effects of 2–4 mM caesium, 10–100 μM ZD-7288 and 1 mM barium on the subthreshold membrane resonance at membrane potentials of $V_0 = -70$ mV, −75 mV and −80 mV. The error bars represent 1 S.D.M.

of vMNs from a given age group were pooled (Fig. 6*D*). Both the amplitude and phase of the impedance of vMNs could be fitted satisfactorily by the above equation with $\tau_m = 13$ ms and $\rho = 20$ for young vMNs and $\tau_m = 35$ ms and $\rho = 20$ for vMNs from newborn animals (Table 2).

The second circuit model makes use of the above estimation of τ_m and ρ (Jack *et al.* 1983) but replaces the semi-infinitely long cable with a single, close-ended cable of length L. The value of L, in multiples of the underlying electrotonic length, λ, can be found from measurements of the change in membrane voltage in responses to injections of current steps. When ρ is large, as found above, the voltage change is postulated to be described by a sum of exponential decaying functions, each with a progressively shorter time constant (Rall, 1969). The length is estimated as:

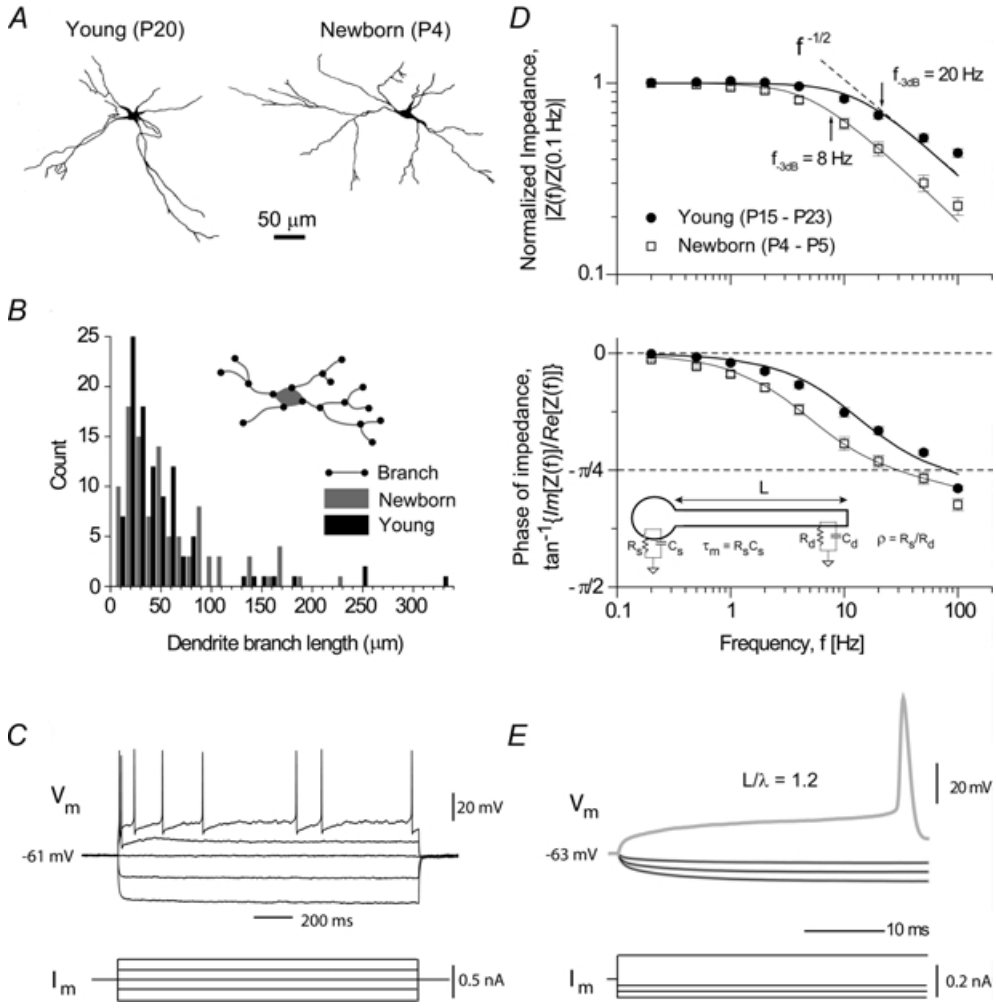

Figure 6. Passive membrane properties of vMNs

A, camera lucida drawings of biocytin-filled vMNs from P20 and P4 animals. *B*, distribution of branch length in vMNs from newborn and young vMNs. *C*, responses to 1 s current step inputs (200 pA steps) in a patch-clamped vMN from a P19 animal. Notice the presence of subthreshold oscillations between spikes, and the absence of hyperpolarization-induced voltage sags. *D*, normalized amplitude (top plot) and phase (bottom plot) of the membrane impedance of vMNs from young (P17 to P23) and newborn (P3 to P5) animals. The impedance was determined in current-clamp mode in the whole-cell patch clamping recording configuration. Continuous lines are fits using the expression for $Z(f)$; see text. Note the logarithmic scale for the normalized amplitude of the membrane impedance. The dotted line labelled $f^{-1/2}$ represents the expected decrease in membrane impedance with higher frequencies for an infinite cable. *E*, averaged subthreshold responses to 300 ms current step injections (40 pA steps) in the same cell as in *C*. Each trace (grey line), except the one featuring an action potential, is the average of 10 recordings. The black lines are dual-exponential fits, with $\tau_0 = 7.2 \pm 0.1$ ms and $\tau_1 = 0.9 \pm 0.1$ ms for all three hyperpolarizing currents, yielding $L/\lambda = 1.2$ for this cell.

Table 3. Gross morphological characteristics of vMNs (means ± S.E.M.)

	Newborn	Young
Sample size	7	5
Soma long axis[1] (μm)	29 ± 3	28 ± 2
Soma short axis[1] (μm)	15 ± 2	16 ± 2
Number of primary dendrites[2]	4–7	5–6
Average dendritic length[3] (μm)	140 ± 30	140 ± 20
Total dendritic length[4] (μm)	840 ± 220	900 ± 250

With respect to diagram: [1]The soma is fit with an ellipse with major and minor axes a and b, respectively. [2]Primary dendrites are labelled l_1 through l_4. [3]The average length (soma to distal end) across all dendrites is $[l_1 + l_2 + l_3 + (l_4 + l_{41}) + (l_4 + l_{42})]/5$. [4]Total dendritic length is $l_1 + l_2 + l_3 + l_4 + l_{41} + l_{42}$.

$$\frac{L}{\lambda} = \pi\sqrt{\frac{\tau_1}{\tau_0 - \tau_1}}$$

given as equation 7.82 in Jack *et al.* (1983), where τ_0 and τ_1 are the dominant and second largest time constants of the exponential fit, respectively. To determine L, we measured the change in voltage in response to injecting 300 ms long current steps over the range of amplitudes from −1.5 to 1.5nA. When action potentials were not elicited, the resultant voltage traces were essentially symmetrical with respect to the resting potential of the cell (Fig. 6*E*), which indicated that no voltage-activated channels were activated by our current steps. The subthreshold voltage response, averaged over 10 trials, could be well fitted with the sum of two exponentials, from which we deduced a value of $L/\lambda = 1.1 \pm 0.2$ for young vMNs and $L/\lambda = 1.4 \pm 0.3$ for newborn vMNs. In summary, the values for ρ and L indicate that the passive characteristics of vMNs are dominated by the impedance of their dendrites.

Suprathreshold resonance

Our final investigation in vMNs dealt with their spiking output in response to sinusoidal current injection. To ascertain the nature of the resonance in the spike rate for vMNs, we injected suprathreshold sinusoidal currents from a membrane potential of $V_0 = -65$ mV and limited the sinusoidal current intensity to be less than 1 nA to prevent damage to the neurones. By way of example, injection of suprathreshold sinusoidal currents in vMNs for either young (Fig. 7*A*) or newborn (Fig. 7*B*) animals elicited multiple spikes per cycle at $f = 0.2$ Hz and 1–2 spikes per cycle at $f = 4$ Hz. We performed a comprehensive set of measurements with sinusoidal input currents that ranged in frequency from 0.2 to 100 Hz and in peak amplitude from 0.6 to 0.9 nA ($n = 10$–13 cells per data point). The average spike rate for all currents showed a clear peak near 20 Hz (Fig. 7*C*; data for higher currents not shown). The relative amplitude of this peak is significantly larger ($P < 0.05$) in young vMNs than in vMNs from newborn animals (Fig. 7*C*). Thus the greater spike rate at the peak of the resonance, i.e. ∼12 spikes s^{-1} in young vMNs *versus* ∼6 spikes s^{-1} in newborn vMNs, correlates with the onset of the subthreshold resonance.

Subthreshold resonance in hypoglossal motoneurones

To assess whether the development regulation of resonance in vibrissa motoneurones is similar in other cranial motoneurones, we measured the subthreshold membrane impedance as a function of frequency in cells from the hypoglossal (XII) nucleus in slices from newborn (P9 to P11) and young (P17 to P21) rats. Visually identified hypoglossal neurones were presumably motoneurones, since this class of cells accounts for the vast majority of neurones in the hypoglossal nucleus (Travers, 1995). Cells that were recorded with sharp electrodes had a resting potential of −62 ± 1 mV and an input resistance of 25 ± 2 MΩ ($n = 23$). In all putative hypoglossal motoneurones, prominent voltage sags and occasional afterhypolarization spikes could be recorded during and after injection of hyperpolarizing currents (Fig. 8*A*). Hypoglossal cells from newborn rats exhibited a subthreshold resonance, defined as $Q \geq 1.05$, at all membrane voltages tested from −60 mV to −80 mV ($Q = 1.15$ at −80 mV) (Fig. 8*B*, right panel). The maximal value of the membrane impedance at 4 Hz in newborn hypoglossal neurones was significantly larger than the corresponding one in newborn vibrissa motoneurones ($P < 0.005$–0.05 for all membrane potentials tested). The amplitude of the resonance substantially increased during development from newborn to young, reaching a value of $Q = 1.35$ (Fig. 8*B*). As in newborn rats, this resonance was also observed at all membrane potentials studied (Fig. 8*B*). In slices from young rats, the subthreshold resonance at −75 mV in hypoglossal motoneurones extended up to 37 ± 6 Hz, a bandwidth significantly larger than that of vibrissa motoneurones, which extended to 19 ± 2 Hz ($P < 0.02$; Figs 3*B* and 8*B*).

Discussion

We have shown that with maturation, vibrissa motoneurones become less excitable by steady-state inputs (Fig. 2) but more sensitive to inputs given in a band of preferred frequencies (Figs 3 and 7). This membrane resonance is absent in animals aged 11 days postnatal and younger, but strong in young animals, aged 17 days postnatal and older. The resonance results from the conjunction of a hyperpolarization-activated cationic current, I_h (Figs 4 and 5), whose slow kinetics preferentially amplify inputs at high frequencies, and the cable properties of vMN dendrites, which attenuate inputs at high frequencies (Fig. 6). We further show that the subthreshold resonant behaviour in vMNs is correlated with a developmentally regulated, tuned response in the spike rate (Fig. 7). The onset and characteristics of the subthreshold membrane resonance in vibrissa motoneurones are features not common to all cranial motoneurones (Fig. 8). We find it of interest that the onset of the resonance in vMNs occurs concomitant with the onset of exploratory whisking.

Suprathreshold responses

In all age groups, the firing pattern of vMNs in response to a step current injection typically consisted of an initial doublet followed by a train of spikes (Fig. 2*A*). Similar dynamics are described for a variety of other motoneurones (Rekling *et al.* 2000). Further, the excitability of vMNs determined as the slope of the *f–I* curve (Fig. 2*C*) decreased from newborn to young animals (Fig. 2*C*). This phenomenon is also seen in hypoglossal neurones (Viana *et al.* 1995). However, in contrast with these cells (Viana *et al.* 1995), we never observed in vMNs an acceleration of the firing rate during a step depolarization (Fig. 2).

Ionic basis of the subthreshold resonance

Three classes of currents may be considered for the resonance in vMNs (Hutcheon *et al.* 1996). The first one involves currents that increase with depolarization, but those can be excluded since the resonance in young vMNs increases with hyperpolarization (Fig. 3). The second class consists of caesium- and barium-sensitive inward potassium currents, which are particularly prevalent in motoneurones. However, these potassium channels can be excluded since barium does not reduce the amplitude of the resonance in young vMNs (Fig. 5). The final class of current includes the hyperpolarization-activated cationic current I_h. At the molecular level, *in situ* hybridization of HCN (hyperpolarization-activated, cyclic nucleotide-gated channel mediating I_h) mRNAs revealed that the facial nucleus has one of the highest concentration of all known HCN channel mRNAs in the entire brain, particularly for the HCN1 and HCN4 channels (Monteggia *et al.* 2000).

Voltage sags in response to injection of hyperpolarizing currents are a hallmark of I_h in facial motoneurones (Larkman *et al.* 1989; Larkman & Kelly, 1992) and their fractional amplitude, measured as a sag ratio, provides a crude estimate of the amplitude of I_h currents in current-clamp mode. Comparisons of sag ratios in different cells

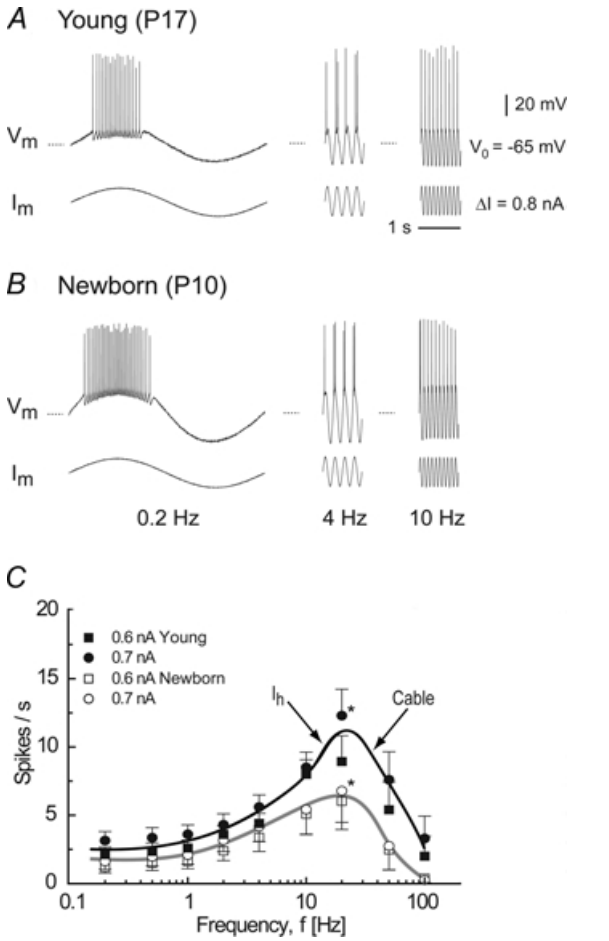

Figure 7. Suprathreshold responses of vMNs from P17 to P23 and P4 to P11 animals in response to sinusoidal current injection
A, membrane potentials of a vMN from a P17 rat during injection of suprathreshold sinusoidal currents with amplitude of 0.8 nA and frequencies of 0.2, 4.0, and 10.0 Hz. *B*, membrane potentials of a vMN from a P10 rat during injection of suprathreshold sinusoidal currents. *C*, the spike rate as a function of stimulus frequency in both vMNs from P17 to P23 and P4 to P11 animals for 0.6–0.7 nA suprathreshold sinusoidal currents. The error bars represent 1 S.E.M. Note the heightened resonance for the P17 to P23 animals; the asterisk signifies that the amplitude of the resonance is significantly higher for P17 to P23 *versus* P4 to P11 animals.

groups have to be taken with caution, but in our case, sag ratios in newborn vMNs may be slightly overestimated compared to those in young vMNs. This systematic bias occurs since the input resistance in newborn vibrissa motoneurones is larger than that in young cells (Table 2) and thus the same current injection results in a larger hyperpolarization in newborn motoneurones (data not shown). Nonetheless, we suggest that the developmental increase in the fractional amplitude of the voltage sag (Fig. 4*B*) reflects an even more pronounced increase in the density of I_h channels from newborn to young animals. It is quite possible that the amplitude of the resonance in adult animals could grow larger than the value we report in young rats that are only starting to whisk. Lastly, the developmental up-regulation of I_h in hypoglossal motoneurones (Bayliss *et al.* 1994) is probably responsible for the increase in subthreshold membrane resonance in these motoneurones (Fig. 8*B*).

Pharmacological blockage of I_h indicates that this current is necessary for the resonance in young vMNs (Fig. 5). Further, the data of Fig. 4*C* and *D* support our contention that the overall density of I_h channels is positively correlated with the presence of subthreshold membrane resonance in vMNs. Yet, the low correlation between resonance and sag suggests that presence of I_h by itself is not sufficient to induce resonance in vibrissa motoneurones. In addition, the activation time constant of the channels, τ_h, must be larger than the time constant of the passive membrane, τ_m (Hutcheon & Yarom, 2000). When both conditions are realized, the resonant frequency, if a resonance exists, lies between $(2\pi\tau_h)^{-1}$ and $(2\pi\tau_m)^{-1}$. Our estimates of sag decays are consistent with the kinetics of I_h, that, in adult facial motoneurones, has a voltage-dependent activation time constant τ_h increasing from 100 to 400 ms for voltages ranging from −115 mV to −85 mV (Larkman & Kelly, 1992).

Electrotonic properties

The observed decrease in membrane impedance at high frequencies was inconsistent with electrically compact vMNs (Fig. 3*B*). Instead of interpreting this low-pass filtering using a compartmental model, we relied on a simple 'ball-and-stick' model (Rall, 1960). The measurement of the concomitant cable properties requires the use of patch microelectrodes because sharp electrode impalements produce a substantial somatic shunt (Table 2). To circumvent the problem of penetrating with patch electrodes the dense neuropil that surrounds facial motoneurones from animals older than P14 (Larkman & Kelly, 1995), we used a mild enzymatic treatment in slices from young rats that conserved the integrity of the slice.

Passive cables have a membrane impedance whose magnitude decreases like the reciprocal of the square root of the frequency, i.e. $|Z| \approx 1/\sqrt{f}$, and whose phase approaches $-\pi/4$ radians at high frequencies. This prediction was verified in vMNs (Fig. 6*D*). Our estimates of the ratio between the conductance of the dendrites and that of the soma and of the electrotonic length indicate that at all ages, the passive membrane properties of vibrissa

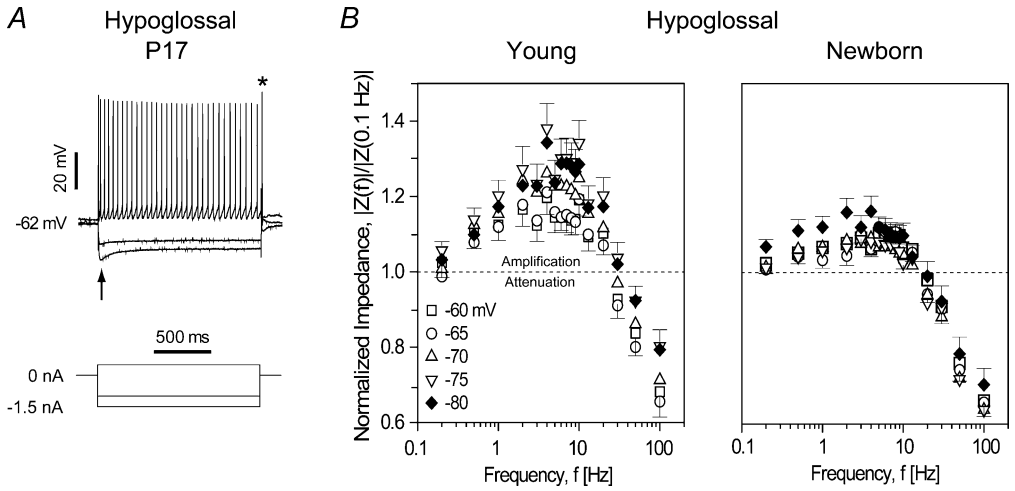

Figure 8. Voltage dependence and developmental regulation of hypoglossal motoneurone resonance
A, subthreshold and suprathreshold responses in a P17 hypoglossal motoneurone elicited by hyperpolarizing and depolarizing current pulses. Notice the voltage sag shortly after the onset of hyperpolarizing current pulse (arrow) and the spike generated during the rebound following repolarization (asterisk). *B*, normalized membrane impedance of hypoglossal neurones from young (P17 to P21) and newborn (P9 to P11) rats. Each data point is the average of 8–12 cells.

motoneurones are dominated by that of their dendrites. These properties shape the decrease of the membrane impedance at high frequencies.

Subthreshold and suprathreshold resonances

Simulations in model neurones have shown, in a rather counter-intuitive manner, that an I_h-based subthreshold resonance induces a suprathreshold resonance having a higher peak frequency (Richardson *et al.* 2003). This theoretical finding corroborates our results showing that the subthreshold resonance in young vMNs peaks at 4 Hz (Fig. 3*B*), at the low end of the range of whisking frequencies, while the resonance in the spiking rate peaks closer to 20 Hz (Fig. 7*C*), at the high end of the whisking range. It is speculated that, *in vivo*, the peak frequency for the spiking resonance drops towards that of the subthreshold resonance in the presence of intracellular noise, as may be caused by high variability in the convergent synaptic inputs to neurones (Richardson *et al.* 2003). A final point is that the frequencies we measured were obtained at $T = 32^{\circ}$C, and an increase to $T = 37^{\circ}$C was shown to almost double the value for the peak frequency of an I_h-based resonance (Hu *et al.* 2002; Uhlrich, 2002).

Specificity of the subtreshold membrane resonance in vMNs

The appearance of the subthreshold resonance in vMNs by the time whisking appears could have been merely coincidental, or even a general feature of cranial motoneurones. To alleviate this concern, we recorded from hypoglossal cells in slices from newborn and young rats. Caudal hypoglossal cells discharge spontaneously at an average rate of 23 Hz (Yang *et al.* 1997) and hypoglossal motoneurones are endowed with developmentally regulated I_h channels (Bayliss *et al.* 1994). It was therefore not surprising to observe a membrane resonance in these cells. However, the subthreshold membrane resonance in hypoglossal cells differed from that in vibrissa motoneurones in three key aspects. First, membrane resonance was observed in hypoglossal motoneurones from newborn animals, at an age when vibrissa motoneurones did not exhibit a resonance. Second, the hypoglossal membrane resonance had a bandwidth twice as wide as that of the resonance in vMNs. Finally, the membrane resonance was present in newborn and young hypoglossal cells at membrane potentials more positive than −65 mV, at variance with the membrane resonance in young vMNs. The last point suggests distinct biophysical mechanisms to generate membrane resonance in hypoglossal and vibrissa motoneurones.

Functional relevance of membrane resonance in vibrissa motoneurones

Although electrical resonance has been found in a variety of mammalian central neurones, the functional relevance of this phenomenon is still in question (Hutcheon & Yarom, 2000). Our results suggest that the broad nature of the membrane resonance in vMNs in animals that whisk encompasses the distribution of whisking frequencies that are exhibited by adult animals (Table 1; left panel, Fig. 3*B*). Conversely, the membrane properties act to attenuate signals across the distribution of whisking frequencies in young animals that are too young to whisk (right panel, Fig. 3*B*). The simultaneous onset of a membrane resonance in vMNs and the appearance of rhythmic whisking support the notion that resonant membrane properties enhance this rhythmic behaviour by preferentially amplifying input signals that are in the range of exploratory whisking while attenuating signals that are outside this range. This selective gain can insure smooth transitions when the control of vibrissa movement is switched between brain centres at multiple levels in the vibrissa sensorimotor pathway.

Resonance in membrane electrical properties has been advanced as a means to synchronize populations of neurones (Izhikevitch, 2001; Richardson *et al.* 2003). This hypothesis is particularly relevant for brainstem nuclei that control rhythmic orofacial behaviours, including chewing, licking, sniffing, and whisking, which may be performed in synchrony under specific circumstances. For the case of licking and whisking, direct projections from interneurones in the hypoglossal nucleus to the facial nucleus (Popratiloff *et al.* 2001) and the existence of a membrane resonance in both nuclei give credence to this hypothesis.

References

Aghajanian GK & Rasmussen K (1989). Intracellular studies in the facial nucleus illustrating a simple new method for obtaining viable motoneurons in adult rat brain slices. *Synapse* **3**, 331–338.

Bayliss DA, Viana F, Bellingham MC & Berger AJ (1994). Characteristic and postnatal development of a hyperpolarization-activated inward current in rat hypoglossal motoneurons in vitro. *J Neurophysiol* **71**, 119–128.

Berg RW & Kleinfeld D (2003). Rhythmic whisking by rat: Retraction as well as protraction of the vibrissae is under active muscular control. *J Neurophysiol* **89**, 104–117.

Budde T, White JA & Kay AR (1994). Hyperpolarization-activated Na^+-K^+ current (I_h) in neocortical neurons is blocked by external proteolysis and internal TEA. *J Neurophysiol* **72**, 2737–2742.

Carvell GE & Simons DJ (1995). Task- and subject-related differences in sensorimotor behavior during active touch. *Somatosens Mot Res* **12**, 1–9.

Carvell GE & Simons DJ (1996). Abnormal tactile experience early in life disrupts active touch. *J Neurosci* **16**, 2750–2757.

Carvell GE, Simons DJ, Lichtenstein SH & Bryant P (1991). Electromyographic activity of mystacial pad musculature during whisking behavior in the rat. *Somatosens Mot Res* **8**, 159–164.

Durand D (1984). The somatic shunt cable for neurons. *Biophys J* **46**, 645–653.

Fee MS, Mitra PP & Kleinfeld D (1997). Central versus peripheral determinants of patterned spike activity in rat vibrissa cortex during whisking. *J Neurophysiol* **78**, 1144–1149.

Friauf E (1986). Morphology of motoneurons in different subdivisions of the rat facial nucleus stained intracellularly with horseradish peroxidase. *J Comp Neurol* **253**, 231–241.

Gao P, Bermejo R & Zeigler HP (2001). Whisker deafferentation and rodent whisking patterns: behavioral evidence for a central pattern generator. *J Neurosci* **21**, 5374–5380.

Hamada Y, Miyashita E & Tanaka H (1999). Gamma-band oscillations in the 'Barrel Cortex' precede rat's exploratory whisking. *Neuroscience* **88**, 667–671.

Hattox AM, Priest CA & Keller A (2002). Functional circuitry involved in the regulation of whisker movements. *J Comp Neurol* **442**, 266–276.

Hu H, Vervaeke K & Storm JF (2002). Two forms of electrical resonance at theta frequencies, generated by M-current, h-current and persistent Na^+ current in rat hippocampal pyramidal cells. *J Physiol* **545**, 783–805.

Hutcheon B, Miura RM & Puil E (1996). Models of subthreshold membrane resonance in neocortical neurons. *J Neurophysiol* **76**, 698–714.

Hutcheon B & Yarom Y (2000). Resonance, oscillation and the intrinsic frequency preferences of neurons. *Trends Neurosci* **23**, 216–222.

Izhikevitch EM (2001). Resonate-and-fire neurons. *Neural Networks* **14**, 883–894.

Jack JJB, Noble D & Tsien RW (1983). *Electrical Current Flow in Excitable Cells*, 2nd edn. Oxford University Press, Oxford.

Kleinfeld D, O'Connor SM & Berg R (1999). Anatomical loops and their relation to electrical dynamics in relation to whisking by rat. *Somatosen Mot Res* **16**, 69–88.

Larkman PM & Kelly JS (1992). Ionic mechanisms mediating 5-hydroxytryptamine- and noradrenaline-evoked depolarization of adult rat facial motoneurones. *J Physiol* **456**, 473–490.

Larkman PM & Kelly JS (1995). The use of brain slices and dissociated neurones to explore the multiplicity of actions of 5-HT in the central nervous system. *J Neurosci Meth* **59**, 31–39.

Larkman PM & Kelly JS (1998). Characterization of 5-HT-sensitive potassium conductances in neonatal rat facial motoneurones *in vitro*. *J Physiol* **508**, 67–81.

Larkman PM & Kelly JS (2001). Modulation of the hyperpolarization-activated current, I_h, in rat facial motoneurones in vitro by ZD-7288. *Neuropharmacol* **40**, 1058–1072.

Larkman PM, Penington NJ & Kelly JS (1989). Electrophysiology of adult rat facial motoneurones: the effects of serotonin (5-HT) in a novel in vitro brainstem slice. *J Neurosci Meth* **28**, 133–146.

Magariños-Ascone C, Núñez Á & Delgado-García JM (1999). Different discharge properties of rat facial nucleus motoneurons. *Neurosci* **94**, 879–886.

Major G, Larkman AU, Jonas P, Sakmann B & Jack JJB (1994). Detailed passive cable models of whole-cell recorded CA3 pyramidal neurons in rat hippocampal slices. *J Neurosci* **14**, 4613–4638.

McCall RB & Aghajanian GK (1979). Serotonergic facilitation of facial motoneuron excitation. *Brain Res* **169**, 11–27.

Mehta SB & Kleinfeld D (2004). Frisking the whiskers: Patterned sensory input in the rat vibrissa system. *Neuron* **41**, 181–184.

Miyashita E, Keller A & Asanuma H (1994). Input-output organization of the rat vibrissal motor cortex. *Exp Brain Res* **99**, 223–232.

Monteggia LM, Eisch AJ, Tang MD, Kaczmarek LK & Nestler EJ (2000). Cloning and localization of the hyperpolarization-activated cyclic nucleotide-gated channel family in rat brain. *Mol Brain Res* **81**, 129–139.

Nicolelis MA, Baccala LA, Lin RC & Chapin JK (1995). Sensorimotor encoding by synchronous neural ensemble activity at multiple levels of the somatosensory system. *Science* **268**, 1353–1358.

O'Connor SM, Berg RW & Kleinfeld D (2002). Coherent electrical activity between vibrissa sensory areas of cerebellum and neocortex is enhanced during free whisking. *J Neurophysiol* **87**, 2137–2148.

Popratiloff AS, Streppel M, Gruart A, Guntinas-Lichius O, Angelov DN, Stennert E, Delgado-Garcia JM & Neiss WF (2001). Hypoglossal and reticular interneurons involved in oro-facial coordination in the rat. *J Comp Neurol* **433**, 364–379.

Rall W (1960). Membrane potential transients and membrane time constant of motoneurons. *Exp Neurol* **2**, 503–532.

Rall W (1969). Time constants and electrotonic length of membrane cylinders and neurons. *Biophys J* **9**, 1483–1508.

Rekling JC, Funk GD, Bayliss DA, Dong X-W & Feldman JL (2000). Synaptic control of motoneuronal excitability. *Physiol Rev* **80**, 767–852.

Richardson MJ, Brunel N & Hakim V (2003). From subthreshold to firing-rate resonance. *J Neurophysiol* **89**, 2538–2554.

Semba K & Komisaruk BR (1984). Neural substrates of two different rhythmical vibrissal movements in the rat. *Neurosci* **12**, 761–774.

Takahashi T (1990). Membrane currents in visually identified motoneurones of neonatal rat spinal cord. *J Physiol* **423**, 27–46.

Takahashi T, Hori T, Kajikawa Y & Tsujimoto T (2000). The role of GTP-binding protein activity in fast central synaptic transmission. *Science* **289**, 460–463.

Thurbon D, Lüscher HR, Hofstetter T & Redman SJ (1998). Passive electrical properties of ventral horn neurons in rat spinal cord. *J Neurophysiol* **79**, 2485–2502.

Travers JB (1995). Oromotor nuclei. In *The Rat Nervous System*, 2nd edn, ed.Paxinos G, pp. 239–256. Academic Press, San Diego.

Turner DA & Schwartzkroin PA (1983). Electrical characteristics of dendrites and dendritic spines in intracellularly stained CA3 and dentate hippocampal neurons. *J Neurosci* **3**, 2381–2394.

Uhlrich D (2002). Dendritic resonance in rat neocortical pyramidal cells. *J Neurophysiol* **87**, 2753–2759.

Viana F, Bayliss DA & Berger AJ (1994). Postnatal changes in rat hypoglossal motoneuron membrane properties. *Neurosci* **59**, 131–148.

Viana F, Bayliss DA & Berger AJ (1995). Repetitive firing properties of developing rat brainstem motoneurones. *J Physiol* **486**, 745–761.

Welker WI (1964). Analysis of sniffing in the albino rat. *Behaviour* **12**, 223–244.

Yang CCH, Kuo TBJ & Chan SHH (1997). Functional characterization of caudal hypoglossal neurons by spectral patterns of neuronal discharges in the rat. *Neurosci* **77**, 813–827.

Acknowledgements

We are grateful to S. du Lac for introducing us to brainstem slice methods, B. Friedman and S. Hefler for assistance with histology, and R. W. Berg, K. Ganguly, D. Golomb, and S. B. Metha for useful discussions. This work was supported by NIH grant MH59867.